Materials & Design 219 (2022) 110754

Contents lists available at ScienceDirect

Materials & Design

journal homepage: www.elsevier.com/locate/matdes

Multiscale modeling of viscoelastic behavior of unidirectional composite laminates and deployable structures

Ning An [a,b,*], Qilong Jia [b], Hao Jin [b], Xiaofei Ma [c], Jinxiong Zhou [b]

[a] School of Aeronautics and Astronautics, Sichuan University, Chengdu 610065, People's Republic of China
[b] State Key Laboratory for Strength and Vibration of Mechanical Structures and School of Aerospace, Xi'an Jiaotong University, Xi'an 710049, People's Republic of China
[c] Xi'an Institute of Space Radio Technology, Xi'an 710100, People's Republic of China

HIGHLIGHTS

- A multiscale approach for modeling viscoelastic composite laminates is developed.
- Abaqus plug-in predicts viscoelastic properties of unidirectional composites.
- Simulation shows effect of stowage on deployment dynamics of a composite hinge.

GRAPHICAL ABSTRACT

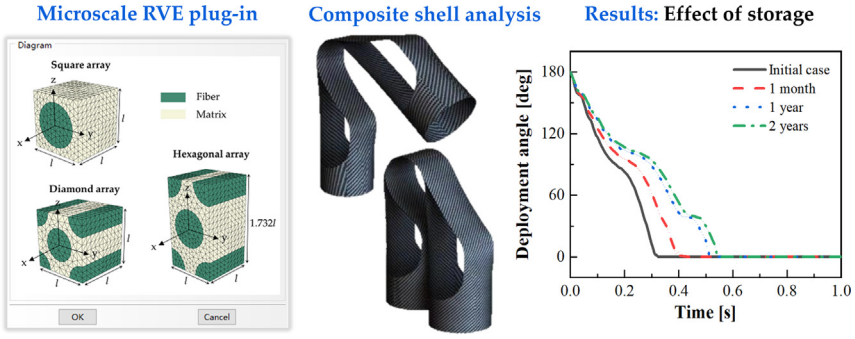

ARTICLE INFO

Article history:
Received 8 January 2022
Revised 25 April 2022
Accepted 12 May 2022
Available online 18 May 2022

Keywords:
Multiscale modeling
Viscoelastic relaxation
Composite laminates
Deployable structures

ABSTRACT

Due to the inherent viscoelasticity of constituent matrix and the possibility of long-term storage, space deployable structures made of composites are likely to exhibit relaxation in the stored strain energy, which may degrade their deployment performance. This paper presents a bottom-up finite element based multiscale computational strategy that bridges the experimentally measurable properties of constituent fibers and matrix to numerical predictions of viscoelastic behavior of composite laminates and general shell structures. A user-friendly RVE analysis plug-in tool is developed in Abaqus/CAE to rapidly estimate the effective orthotropic viscoelastic properties of unidirectional composites by taking as input the microstructure geometry as well as the known properties of fibers and matrix. Some benchmark problems were solved, and the accuracy and efficiency of the proposed plug-in tool were verified. Next, the strategy is shown to be applicable to model the viscoelastic behavior of macroscale composite laminates and deployable shell structures, by utilizing built-in functions in Abaqus to define the stacking sequence and accordingly update the material properties. In particular, the proposed multiscale strategy was employed to simulate the influence of modulus relaxation on the deployment dynamics of a composite tape-spring hinge, and good agreement was achieved as compared to reported experimental results.

1. Introduction

Advanced composite laminates and deployable structures are of increasing interest for the design of large-scale functional systems in the aerospace industry as they provide much higher modulus-to-mass ratio and wider range of shapes that can be fabricated at

* Corresponding author at: School of Aeronautics and Astronautics, Sichuan University, Chengdu 610065, People's Republic of China.
E-mail address: anning@scu.edu.cn (N. An).

https://doi.org/10.1016/j.matdes.2022.110754
0264-1275/

low cost than their metallic counterparts. These composite laminated structures are often thin-walled, designed to be elastically folded or flattened and then coiled for storage before and during launch, and capable of deploying spontaneously by releasing the stored strain energy for use once in orbit [1–4]. Fig. 1 presents the deployed and folded configurations of two typical composite deployable structures, i.e., the composite tape-spring hinge (CTSH) and the composite thin-walled lenticular tube (CTLT).

Due to the specific application scenario in aerospace, before use, composite deployable structures are often stored for extended periods (on the order of months or even years), while being exposed to a serve thermal condition in the space environment [5,6]. During the long-term storage in spacecraft, the deployable structures are subjected to a constant deformation/strain that causes substantial stress relaxation due to the viscoelasticity of constituent polymers, which may lead to a reduction in the stored strain energy and ultimately produce an impact on their deployment performance [7]. A series of experimental tests have been conducted recently by NASA under a Game Changing Development Program (GCDP) project to characterize the influence of viscoelastic relaxation on the deployment performance of composite deployable boom structures [8–10]. It is reported that the deployment performance of composite structures will degrade obviously during storage until at one point that the structure will entirely fail to deploy, and the variation of environmental temperature also has a significant effect on the degradation of deployment rate. As it is extremely unlikely that the large-scale space structures will not be stowed in a coiled/folded configuration before launching, it is crucial to spacecraft designing to know how long a deployable structure can be stored without causing deployment failure. On the other hand, the viscoelasticity can sometimes be employed as a source of damping for lightweight space structures, and by understanding how the stiffness of composite laminates decreases over time, a spacecraft engineer who attempts to slow down the deployment can then know how long and at what temperature to store the structures to obtain a desirable performance [11–15].

Several studies have been conducted for the purpose of gaining knowledge about the viscoelastic behavior of thin-walled deployable structures made of composite laminates. A rigorous viscoelastic model for general composite structures ought to consist of multiscale modeling techniques, which from bottom to top are known as the RVE analysis at micro-level, the calculation of ABD matrix at meso-level, and the simulation of general composite structures at macro-level [17]. Following this strategy, Kwok et al. [18] proposed a general viscoelastic model that efficiently predicts the deployment performance of plain-weave composite tape-spring shells that are deployed after being held folded for a given period of time. A two-step homogenization procedure is applied to determine the relaxation ABD matrix of viscoelastic plane-weave laminate; the first homogenization at microscale deals with determining the effective relaxation properties of composite tows from fiber and matrix properties, and the second homogenization at mesoscale yields the relaxation ABD matrix of the plain-weave laminate. Finally, the relaxation ABD matrix is coded into a user defined shell section subroutine to model the viscoelastic behavior of macroscale general composite shell structures. A similar strategy was also formulated by Liu et al. [19,20] who used mechanics of structure genome (MSG) to predict the viscoelastic behavior of textile composites. For unidirectional crossply laminates, however, the two-step homogenization procedure can be further simplified by avoiding the ABD calculation at mesoscale and bridging the microscale and macroscale analysis via built-in functions in commercial finite element (FE) packages.

Very recently, Fernandes et al. [21] proposed a numerical approach that simulates the viscoelastic relaxation of unidirectional composite laminates by employing the idea of 'fictitious' temperature. The stacking sequence of the laminates is defined by using a composite shell section, and the time-dependent properties for each lamina are correlated to a set of 'fictitious' temperatures. The material properties of the composites could then be updated from an unrelaxed to a relaxed state by inducing a change in the 'fictitious' temperature. This numerical practice provides an advantage over the aforementioned two-step homogenization method because the time-dependent lamina properties are directly used in the macroscale composite structure analysis by utilizing built-in functions in commercial software, thus avoiding the calculation of ABD matrix at mesoscale. In other words, an efficient macroscale viscoelastic model for general laminated shell structures is readily available as long as a microscale RVE analysis is performed and the time-dependent lamina properties are obtained.

A common approach to estimating the effective relaxation properties of viscoelastic composite lamina is to homogenize the properties of the fiber and matrix within a periodic unit cell. Several theoretical homogenization methods are available. For example, analytical closed form expressions for the effective coefficients of fibrous viscoelastic composites are obtained in [22–24] by means of the two-scale Asymptotic Homogenization

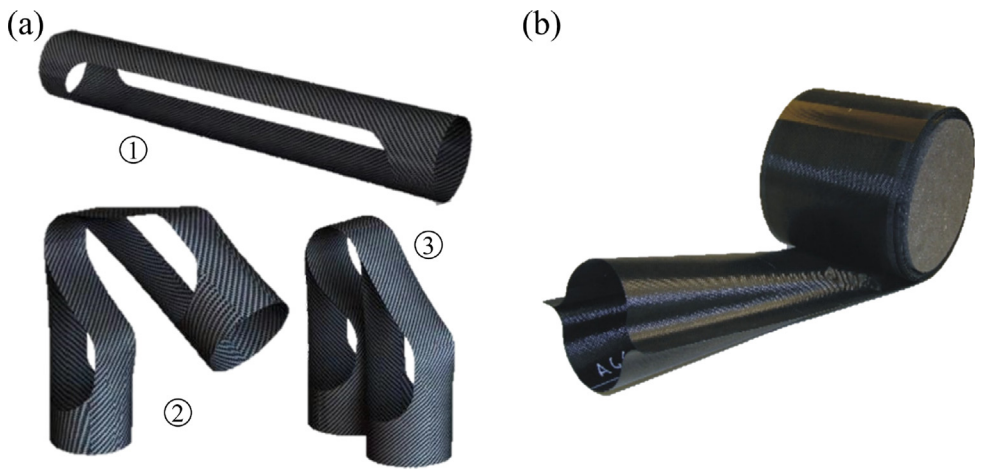

Fig. 1. Notable examples of thin-walled stored strain energy deployable structures made of composite laminates. These structures are elastically folded or coiled for storage before and during launch, and are able to deploy by releasing the stored strain energy for use once in orbit. (a) Composite tape-spring hinge (CTSH) in deployed, partially folded, and fully folded configuration. (b) Composite thin-walled lenticular tube (CTLT) partially coiled around a cylindrical hub, modified from [16].

Method (AHM). Given that analytical solution can only be derived for a few simple composite structures, semi-analytical techniques combing AHM with FEM may be required for analyzing more complex microstructures [25,26]. Besides, the micromechanics-based FE-RVE approach has been used for decades as powerful tools for the same purpose [27–32]. In general, the FE-RVE homogenization approach takes full advantage of powerful functions in commercial FE packages such as ANSYS and ABAQUS, which would facilitate interaction between academia and industry. Moreover, all computations with FE-RVE model could be accomplished directly in the time domain, hence the Laplace transform is not needed in this theory.

For the continuous fiber-reinforced unidirectional composites, it is often assumed that fibers are uniformly distributed in the matrix and the fiber arrangement follows regular, repeated patterns as shown in Fig. 2. We note that although fibers are likely to distribute in a random manner in reality, the implementation of a regular fiber arrangement provides high enough accuracy at low computational cost [33,34]. The basic idea of RVE homogenization is to evaluate the response of a microscale RVE subjected to simple deformation modes such as uniaxial tension and simple shear, and the core of this technique rests on ensuring the external surfaces of the RVE remain periodic in the deformation process, which, requires the implementation of appropriate periodic boundary conditions (PBCs). The implementation of PBCs is achievable in commercial FE packages but generally requires extensive in-house programming [35]; otherwise complex and time-consuming user inputs may be needed. A number of plug-in tools to address this issue have been developed within commercial FE packages to facilitate the set-up, analysis and post-processing of RVE models [36–38], however, most of them have been limited to analyzing the homogenized properties of elastic RVEs.

The main novelty of this work is to develop a user-friendly plug-in tool that provides an easy-to-use, robust and fast technique for users to evaluate the effective relaxation properties of viscoelastic composites, without the need to derive complex formulas. Having obtained the viscoelastic properties of each lamina, we also show how these properties can be used to model the viscoelastic behavior of composite laminates and macroscale deployable shell structures, by utilizing built-in functions in commercial package without further programming work.

Firstly, we establish a constitutive model for viscoelastic unidirectional composites by considering a microscale representative volume element (RVE). A user-friendly interface plug-in tool is developed in Abaqus/CAE to estimate the effective viscoelastic properties of unidirectional composites by taking as input the microstructure geometry as well as the properties of constituent fiber and matrix materials. The interfaces of the tool allow users to automatically create FE-RVE models, run stress relaxation analysis and return the effective properties of the composites as output. The efficiency of the proposed tool was validated by solving some benchmark problems for both elastic and viscoelastic cases. By taking advantage of the plug-in tool, a parametric numerical study has been conducted to investigate the effect of variation in microstructure geometry and environmental temperature on the viscoelastic relaxation of unidirectional composites. We then show that the time-dependent lamina properties output by the plug-in can be subsequently used to model the viscoelastic behavior of composite laminates at macroscale with the help of Abaqus built-in functions to define the stacking sequence and accordingly update the material properties. Specifically, taking the composite tape-spring hinge (CTSH) as an example, we formulated a 3D shell FE model and quantified the effect of long-term stowage on the deployment dynamics of stored strain energy deployable structures. It is shown, in good agreement with previous experimental works, that the long-term stowage would lead to a significant decrease in the deployment rate of the hinge when compared to the unstored case.

The paper is organized as follows. Section 2 presents the theoretical basis for the constitutive model of viscoelastic unidirectional composites. Section 3 describes the development and implementation details of the Abaqus plug-in *Viscoelastic RVE Calculator* and a user-defined material subroutine UMAT for evaluating the effective time-dependent material properties of

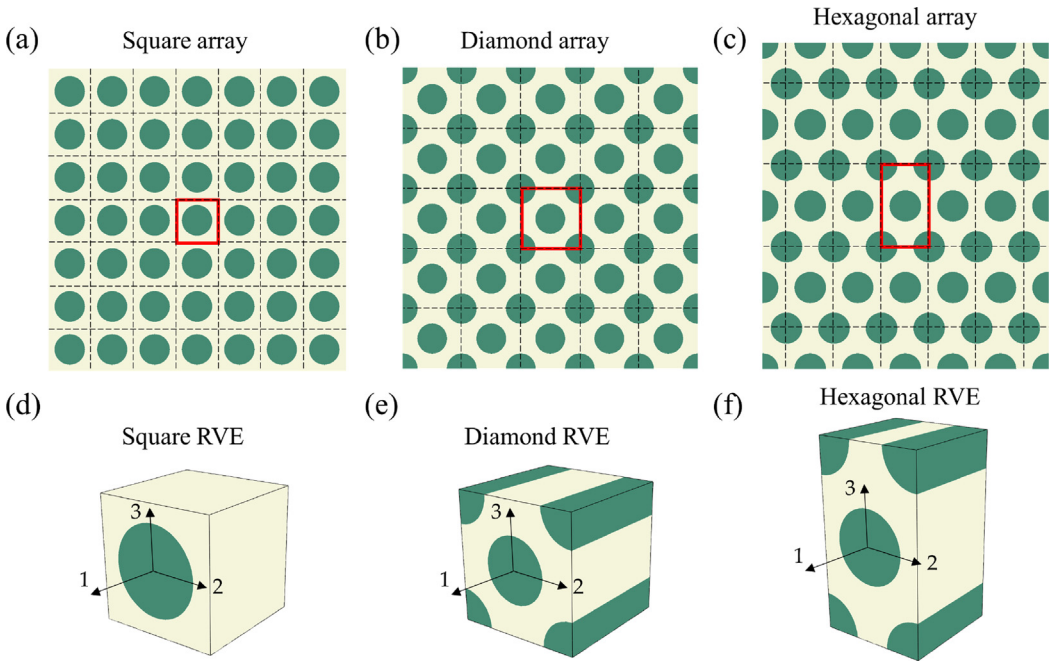

Fig. 2. Geometry of unidirectional composites with regular fiber arrays. Cross-section view of (a) square array, (b) diamond array, and (c) hexagonal array. RVE geometries in (d) square array, (e) diamond array, and (f) hexagonal array.

unidirectional composites by considering a viscoelastic RVE. The efficiency of the proposed tools is verified and validated by solving a series of benchmark problems consist of both elastic and viscoelastic cases in Section 4. In Section 5, a 3D shell model for CTSH is introduced and the simulation results are compared to previously reported experimental data, highlighting the effect of long-term storage on the deployment dynamics of deployable structures. Finally, concluding remarks are included in Section 6.

2. Theoretical basis

2.1. Properties of constituents

The composite materials are made of two phases of constituent materials: fiber reinforcements and polymer matrix. The stress relaxation in composite materials is primarily due to the inherent viscoelasticity of the polymer matrix, since the most commonly used reinforcing fibers are inorganic (e.g., carbon, glass) and their viscosity is negligible. Accordingly, in this work we assume a linear elastic behavior of the fibers, while the polymer matrix is treated as an isotropic and linear viscoelastic material. The viscoelasticity of a material can be characterized by considering a uniaxial tensile test in which a time varying strain $\varepsilon(t)$ is applied to the material. The stress $\sigma(t)$ is then measured as a function of time t as follows [39]:

$$\sigma(t) = \int_0^t E(t-s)\frac{d\varepsilon(s)}{ds}ds \tag{1}$$

where $E(t-s)$ is the time-dependent *relaxation modulus function* that characterizes the material's response. This constitutive behavior can be understood that the value of σ at time t depends on all the values of $\varepsilon(s)$ for s varying from 0 to t.

The expression of $E(t)$ can be experimentally illustrated by considering a relaxation test in which a strain ε is suddenly applied to a specimen and then held constant for a long time. The beginning of the experiment, when then strain is suddenly applied, is taken as zero time, so that

$$\sigma(t) = E(t)\varepsilon^{cst} \quad (\text{since } \dot{\varepsilon} = 0 \text{ for } t > 0) \tag{2}$$

where ε^{cst} is the fixed strain.

A Prony series is commonly used to approximate the relaxation modulus over a wide range of time scales based on the generalized Maxwell model as follows:

$$E(t) = E_\infty + \sum_{i=1}^{n} E_i e^{-\frac{t}{\tau_i}} \tag{3}$$

where E_∞ is the long-term modulus, and E_i and τ_i are the modulus and relaxation time constant of the i-th arm of the generalized Maxwell model. Another equivalent form for the time-dependent relaxation modulus is expressed as

$$E(t) = E_0 - \sum_{i=1}^{n} E_i\left(1 - e^{-\frac{t}{\tau_i}}\right) \tag{4}$$

where E_0 is the instantaneous modulus and $E_0 = E_\infty + \sum_{i=1}^{n} E_i$.

Temperature has a significant effect on the time-dependent behavior of a viscoelastic material. Specifically, a long-time relaxation process of a material at low temperatures is somehow equivalent to a short-time relaxation process at high temperatures. The temperature dependence of the relaxation modulus is correlated to time through the time–temperature superposition principle, in which the relaxation times at two temperatures are related by a shift factor α_T.

$$\alpha_T = \frac{\tau(T)}{\tau(T_0)} \tag{5}$$

A commonly used shift function for α_T is defined by the Williams-Landel-Ferry (WLF) approximation, which takes the following form:

$$\log \alpha_T = -\frac{C_1(T - T_0)}{C_2 + (T - T_0)} \tag{6}$$

where T_0 is the reference temperature at which the relaxation data is given, T is the temperature of interest, and C_1 and C_2 are the calibration constants at the reference temperature.

2.2. Constitutive modeling of unidirectional viscoelastic composites

The unidirectional composites that consist of elastic oriented fibers embedded into an isotropic viscoelastic matrix are generally assumed to be linear, orthotropic and viscoelastic, for which the homogenized macroscopic constitutive equations can be realized by expanding the 1D stress relaxation relation in Eq. 2 to a 3D stress relaxation stiffness matrix relation:

$$\{\overline{\sigma}(t)\} = [C(t)]\{\overline{\varepsilon}^{cst}\} \tag{7}$$

where $[C(t)]$ is the effective relaxation stiffness matrix, and $\{\overline{\sigma}(t)\}$ and $\{\overline{\varepsilon}^{cst}\}$ refer to the macro-stress and macro-strain matrix, the component of which is defined by averaging the heterogeneous stress and strain tensor over the volume of the RVE as given by Eqs. 8 and 9. Periodic boundary conditions are required to ensure the homogenization of the microstructure, and a more detailed description of the governing equations of this problem can be found in the early work of Sun and Vaidya [27].

$$\overline{\sigma}_{ij}(t) = \frac{1}{V}\int_V \sigma_{ij}(x,y,z)\mathrm{d}V \tag{8}$$

$$\overline{\varepsilon}_{ij}(t) = \frac{1}{V}\int_V \varepsilon_{ij}(x,y,z)\mathrm{d}V \tag{9}$$

The component form of the constitutive relation [Eq. 7] can be written as follows using the Voight notations:

$$\begin{bmatrix}\overline{\sigma}_{11}(t)\\ \overline{\sigma}_{22}(t)\\ \overline{\sigma}_{33}(t)\\ \overline{\sigma}_{23}(t)\\ \overline{\sigma}_{31}(t)\\ \overline{\sigma}_{12}(t)\end{bmatrix} = \begin{bmatrix} C_{11}(t) & C_{12}(t) & C_{13}(t) & 0 & 0 & 0\\ C_{12}(t) & C_{22}(t) & C_{23}(t) & 0 & 0 & 0\\ C_{13}(t) & C_{23}(t) & C_{33}(t) & 0 & 0 & 0\\ 0 & 0 & 0 & C_{44}(t) & 0 & 0\\ 0 & 0 & 0 & 0 & C_{55}(t) & 0\\ 0 & 0 & 0 & 0 & 0 & C_{66}(t)\end{bmatrix}\begin{bmatrix}\overline{\varepsilon}_{11}^{cst}\\ \overline{\varepsilon}_{22}^{cst}\\ \overline{\varepsilon}_{33}^{cst}\\ \overline{\gamma}_{23}^{cst}\\ \overline{\gamma}_{31}^{cst}\\ \overline{\gamma}_{12}^{cst}\end{bmatrix} \tag{10}$$

The entries in the relaxation stiffness matrix C_{ij} can be determined through a series of relaxation tests in which a constant macro-strain matrix $\overline{\varepsilon}^{cst}$ is applied to the homogenized RVE and then the macro-stress matrix $\overline{\sigma}(t)$ is measured as a function of time t. For example, in loading case 1, a constant macroscopic strain $\overline{\varepsilon}_{11}^{cst}$ was applied along 1-direction and all the other strains are set to zero, and in this case the $C_{11}(t), C_{12}(t)$ and $C_{13}(t)$ are computed as:

$$C_{11}(t) = \overline{\sigma}_{11}(t)/\overline{\varepsilon}_{11}^{cst}, \quad C_{12}(t) = \overline{\sigma}_{22}(t)/\overline{\varepsilon}_{11}^{cst}, \quad C_{13}(t) = \overline{\sigma}_{33}(t)/\overline{\varepsilon}_{11}^{cst} \tag{11}$$

Consequently, all the relaxation stiffness matrix entries are calculated by considering in total six loading cases as listed in Table 1.

Notice that each entry $C_{ij}(t)$ is a function of time and can be approximated by a Prony series having the same relaxation times as the matrix but different Prony coefficients.

$$C_{ij}(t) = C_{ij,\infty} + \sum_{k=1}^{n} C_{ij,k} e^{-\frac{t}{\tau_i}} = C_{ij,0} - \sum_{k=1}^{n} C_{ij,k}\left(1 - e^{-\frac{t}{\tau_i}}\right) \tag{12}$$

where $C_{ij,\infty}$ and $C_{ij,k}$ are the mechanical parameters to be determined.

Table 1
Estimation of stiffness matrix constants C_{ij} under six loading cases.

Loading case	Calculation of C_{ij}
$\overline{\varepsilon}_{11}=\overline{\varepsilon}_{11}^{cst};\overline{\varepsilon}_{22},\overline{\varepsilon}_{33},\overline{\gamma}_{23},\overline{\gamma}_{31},\overline{\gamma}_{12}=0$	$C_{11}(t)=\overline{\sigma}_{11}(t)/\overline{\varepsilon}_{11}^{cst}, C_{12}(t)=\overline{\sigma}_{22}(t)/\overline{\varepsilon}_{11}^{cst}, C_{13}(t)=\overline{\sigma}_{33}(t)/\overline{\varepsilon}_{11}^{cst}$
$\overline{\varepsilon}_{22}=\overline{\varepsilon}_{22}^{0};\overline{\varepsilon}_{11},\overline{\varepsilon}_{33},\overline{\gamma}_{23},\overline{\gamma}_{31},\overline{\gamma}_{12}=0$	$C_{12}(t)=\overline{\sigma}_{11}(t)/\overline{\varepsilon}_{22}^{cst}, C_{22}(t)=\overline{\sigma}_{22}(t)/\overline{\varepsilon}_{22}^{cst}, C_{23}(t)=\overline{\sigma}_{33}(t)/\overline{\varepsilon}_{22}^{cst}$
$\overline{\varepsilon}_{33}=\overline{\varepsilon}_{33}^{cst};\overline{\varepsilon}_{11},\overline{\varepsilon}_{22},\overline{\gamma}_{23},\overline{\gamma}_{31},\overline{\gamma}_{12}=0$	$C_{13}(t)=\overline{\sigma}_{11}(t)/\overline{\varepsilon}_{33}^{cst}, C_{23}(t)=\overline{\sigma}_{22}(t)/\overline{\varepsilon}_{33}^{cst}, C_{33}(t)=\overline{\sigma}_{33}(t)/\overline{\varepsilon}_{33}^{cst}$
$\overline{\gamma}_{23}=\overline{\gamma}_{23}^{cst};\overline{\gamma}_{31},\overline{\gamma}_{12},\overline{\varepsilon}_{11},\overline{\varepsilon}_{22},\overline{\varepsilon}_{33}=0$	$C_{44}(t)=\overline{\sigma}_{23}(t)/\overline{\gamma}_{23}^{cst}$
$\overline{\gamma}_{31}=\overline{\gamma}_{31}^{cst};\overline{\gamma}_{23},\overline{\gamma}_{12},\overline{\varepsilon}_{11},\overline{\varepsilon}_{22},\overline{\varepsilon}_{33}=0$	$C_{55}(t)=\overline{\sigma}_{31}(t)/\overline{\gamma}_{31}^{cst}$
$\overline{\gamma}_{12}=\overline{\gamma}_{12}^{cst};\overline{\gamma}_{23},\overline{\gamma}_{31},\overline{\varepsilon}_{11},\overline{\varepsilon}_{22},\overline{\varepsilon}_{33}=0$	$C_{66}(t)=\overline{\sigma}_{12}(t)/\overline{\gamma}_{12}^{cst}$

For particular cases where deformation of composites occurs in a short time the viscosity of materials can be neglected, and the constitutive equations (Eqs. 7 and 10) will reduce to conventional elastic orthotropic stress–strain relations. The stiffness matrix $[C]$ would become a constant matrix with each entry defined by the instantaneous value of $C_{ij}(t)$ as follows:

$$C_{ij}=C_{ij,0}=C_{ij,\infty}+\sum_{k=1}^{n}C_{ij,k} \tag{13}$$

The effective engineering constants for elastic unidirectional composites such as $E_1, E_2, v_{12}, v_{23}, G_{12}, G_{23}$ can be finally obtained by correlating each component described as follows:

$$[S]=[C]^{-1}=\begin{bmatrix} \frac{1}{E_1} & -\frac{v_{21}}{E_2} & -\frac{v_{31}}{E_3} & 0 & 0 & 0 \\ -\frac{v_{12}}{E_1} & \frac{1}{E_2} & -\frac{v_{32}}{E_3} & 0 & 0 & 0 \\ -\frac{v_{13}}{E_1} & -\frac{v_{23}}{E_2} & \frac{1}{E_3} & 0 & 0 & 0 \\ 0 & 0 & 0 & \frac{1}{G_{23}} & 0 & 0 \\ 0 & 0 & 0 & 0 & \frac{1}{G_{13}} & 0 \\ 0 & 0 & 0 & 0 & 0 & \frac{1}{G_{12}} \end{bmatrix} \tag{14}$$

where $[S]$ is the compliance matrix, which is defined as the inverse of the stiffness matrix $[C]$.

3. Software methodology and implementation

This section presents the development and implementation details of the Abaqus plug-in *Viscoelastic RVE Calculator* and a user-defined material subroutine *UMAT* for evaluating and simulating the effective relaxation stiffness matrix of viscoelastic unidirectional composites through the microscale RVE approach.

3.1. Structure of the plugin

The plug-in has been developed in Abaqus/CAE 2020, thus users are suggested to use the same or later version to avoid problems executing the plug-in. The python code for the plug-in is available upon reasonable request to the corresponding author, and the installation is simple and intuitive: place the code in the *abaqus_plugins* directory before starting the software. Once successfully installed, in the main menu bar of Abaqus one can find the plug-in *Viscoelastic RVE Calculator* under the tab *Plug-ins*, see Fig. 3.

The plug-in consists of three tabs which cover all stages from pre- to post-processing: it can be used to automatically create the FE-RVE model, assign appropriate material properties to predefined fiber and matrix elements, generate periodic boundary conditions (PBC) and run the stress-relaxation analysis, and return the results as requested. The plug-in provides functionalities for calculating the effective material properties from both elastic RVEs and viscoelastic RVEs. The use of the plug-in with step-by-step procedures and output for calculating elastic and viscoelastic RVEs is presented in Video S1 and S2 in the Supplementary Information.

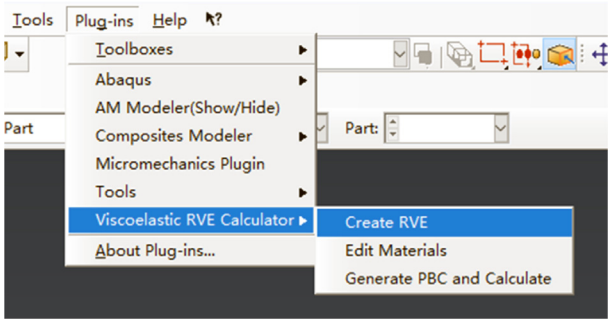

Fig. 3. *Viscoelastic RVE Calculator* plug-in in Abaqus main menu.

1) Create RVE: The first tab of the plug-in is *Create RVE* which provides functionality for defining geometry and finite element mesh of certain types of RVE by specifying a limited number of input parameters. First, the plug-in allows the user to select one from the RVE library of three idealized RVE models characterized by regular fiber arrays. These models in the library are shown in Fig. 3 and include the square array, diamond array and hexagonal array. Note that perfect bonding conditions are assumed at the interface between the matrix and fiber. Next, the user has to input the fiber volume fraction as well as the RVE length (denoted by l) to describe the RVE geometry; the input parameter of edge seeds determines the number of elements across the RVE edge l. By default, the quadratic tetrahedral elements (Abaqus element type C3D10) are employed to automatically discretize the RVE geometry in the plug-in. To ensure the proper implementation of PBC, one eighth of the RVE is created and meshed first, and then it is repeated to generate the full RVE mesh model according to symmetry.

2) Edit materials: The finite elements of the RVE are automatically grouped into two elements sets as fiber and matrix, as indicated by the colors in Fig. 4(a). Next, the user is prompted to assign appropriate material properties to these pre-defined fiber and matrix elements sets. As has been explained in Section 2.1, the fiber is assumed to be linear, elastic, and isotropic or transversely isotropic; while the matrix is modeled as linear, elastic or viscoelastic, and isotropic. These material properties are allowed to be defined directly through Abaqus material module GUI. The *Edit materials* tab, as shown in Fig. 4(b), then could be used to assign the appropriate material properties to the fiber and matrix domain, respectively.

3) Generate PBC and calculate: Fig. 4(c) shows the GUI interface of the last tab *Generate PBC and calculate* of the plug-in, which is developed to automatically generate periodic boundary conditions, successively run the aforementioned six load cases in Table 1, and post-process the calculations to obtain the effective time-dependent relaxation stiffness matrix coefficients. The results are consequently saved in the Abaqus work directory under.csv files. To begin with, the user has to select an applicable RVE model and part to analyze; note that the RVE part should be created with

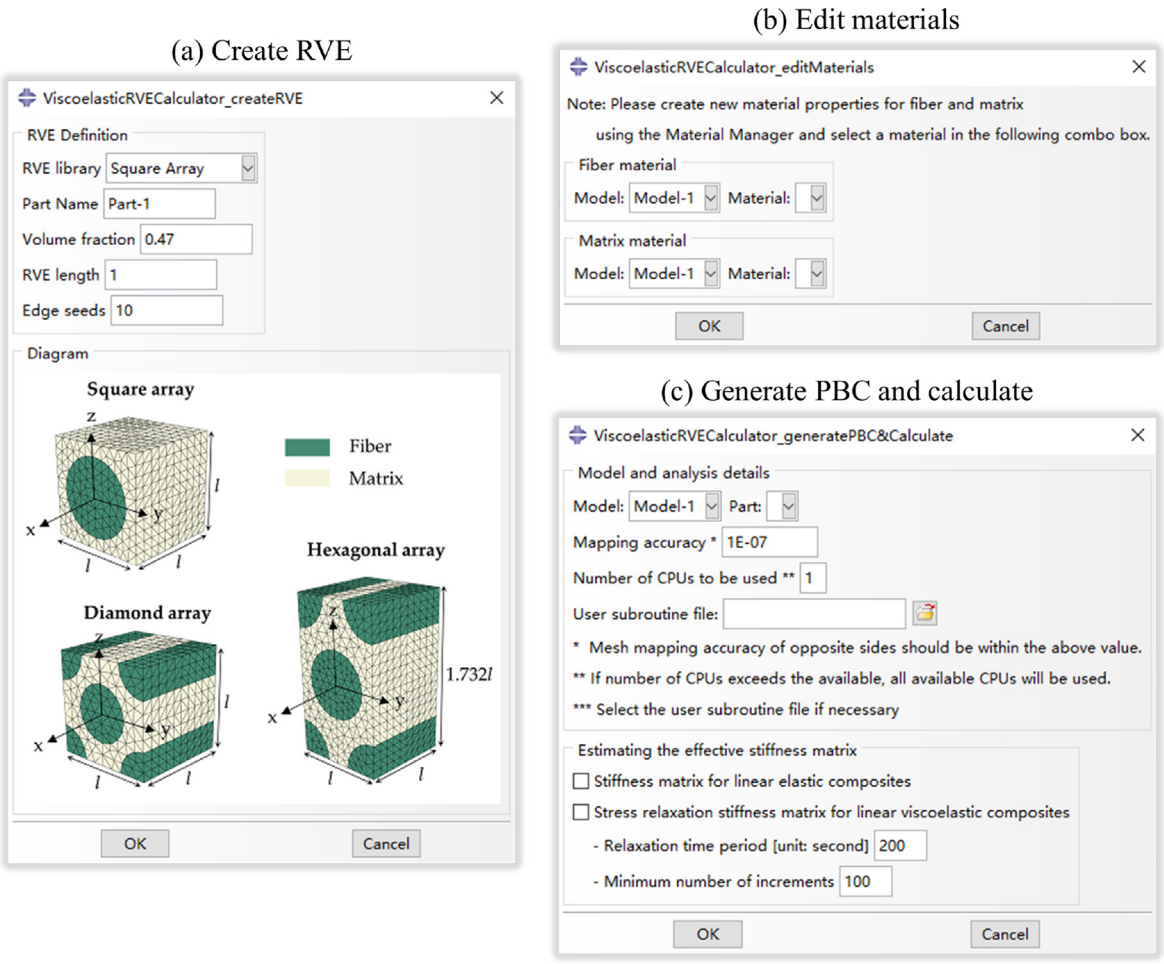

Fig. 4. Tab GUI windows in the plug-in: (a) *Create RVE*, (b) *Edit materials*, and (c) *Generate PBC and calculate*.

the definition of constituent materials' properties and meshing, which can be accomplished either by using the above two tabs or manually in Abaqus GUI. Notice that used in conjunction with other previously developed software programs such as *RVE for composites* [38], this tab could be readily used to predict the effective mechanical properties of composites with even more complex fiber distributions. The user is also allowed to set the mesh mapping accuracy for generating the periodic boundary conditions; we note that the source code of EasyPBC was employed here and more details about the implementation of periodic boundary conditions can be found in the reference [37]. Next, the number of CPUs to use should be specified, and the user subroutine file can be prescribed if required to define the constituent materials' properties. Finally, the last panel *estimating the effective stiffness matrix* provides user two functions to perform: (*i*) if the matrix is treated as a linear elastic material, the constant stiffness matrix coefficients for the orthotropic elastic RVE will be estimated, as well as the corresponding engineering constants; and (*ii*) if the matrix is treated as a linear viscoelastic material, the effective relaxation stiffness matrix coefficients for the orthotropic viscoelastic RVE will be estimated. In the former case, the elastic behavior of RVE is analyzed with linear static analysis (*Static, General in Abaqus) by considering the six loading cases given in Table 1. In the latter case the viscoelastic behavior of RVE is analyzed with two quasi-static visco analysis steps (*Visco in Abaqus). The first step is defined to apply the instantaneous strains, and the second step is developed for holding the applied strains constant for a specified length of simulation time during which the time-dependent stress relaxation response of the viscoelastic RVE is computed. The plug-in allows the user to specify the relaxation time period as well as the minimum number of increments as input parameters to control the time length and interval of data collection.

3.2. Equivalent homogenized model with UMAT

As mentioned above, our plug-in *Viscoelastic RVE Calculator* is capable of adequately evaluating the effective elastic or viscoelastic orthotropic material properties of the unidirectional composites by taking constituents properties as input based on micromechanics approaches. In practice, however, it is unrealistic and computationally inefficient to model every fiber within the matrix in the composites. Alternatively, the macro-level simulations are frequently based on finite element method performed by assuming that the composite structures is composed of multilayer homogeneous materials by assigning homogenized properties to each lamina layer. Unfortunately, the orthotropic material behavior that can be modeled by commercial finite element packages such as Abaqus is restricted to circumstances involving simple elasticity and plasticity but not viscoelasticity. When the matrix is treated as a linear elastic material and the RVE demonstrates orthotropic elastic behavior, the engineering constants such as $E_{11}, E_{22}, E_{33}, \nu_{23}, \nu_{31}, \nu_{12}, G_{23}, G_{31}, G_{12}$ can be defined directly with the built-in functionalities in Abaqus GUI; whereas for modeling the orthotropic relaxation behavior of a viscoelastic RVE, an additional user-defined material subroutine UMAT is needed.

The implementation of UMAT is not complicated since the Jacobian matrix is readily available according to the stress–strain relations in Eq. 10. For small-deformation problems, the consistent Jacobian matrix is defined as:

$$DDSDDE = \frac{\partial \boldsymbol{\sigma}^A}{\partial \boldsymbol{\epsilon}^A} \tag{15}$$

where the superscript $()^A$ denotes a quantity in Abaqus notation. The terms $\boldsymbol{\sigma}^A$ and $\boldsymbol{\varepsilon}^A$ is a 6×1 array, and $DDSDDE$ is a 6×6 matrix. $DDSDDE(I,J)$ defines the change in the Ith stress component caused by an infinitesimal perturbation of the Jth component of the strain increment array. Notice that Abaqus uses a different notation and $DDSDDE(I,J) = C_{IJ}$ holds true, except for two cases where $DDSDDE(4,4) = C_{66}$ and $DDSDDE(6,6) = C_{44}$ [40].

The Abaqus UMAT is developed to compute the homogeneous orthotropic linear viscoelastic behavior of unidirectional composites by using the relaxation stiffness matrix coefficients obtained from RVE analysis as input. Hence, the complex composite structures that consist of multilayer unidirectional lamina can be modeled by defining homogenized viscoelastic properties to each layer by using the UMAT subroutine. This procedure is necessary in order to calculate the ABD matrix of the composite laminates through a second homogenization computation at mesoscale, which is frequently required for the viscoelastic modeling of woven composite structures [18].

4. Numerical examples

4.1. Calculation of effective properties for elastic RVE

We began by calculating the effective properties for elastic RVE by treating both matrix and fiber as linear elastic materials. Although analytical and numerical approaches have been well-established in the literature [27,29] to evaluate the effective elastic properties of unidirectional composites made of elastic matrix and fibers using RVE analysis, here we reproduce the benchmark case to validate the effectiveness of *Viscoelastic RVE Calculator* plug-in and reveal the effect of fiber arrangement on the predictions of effective elastic properties. In this case, the fiber and matrix properties are taken from Ref. [29], in which the authors developed a micromechanical FE-RVE model with a random fiber array. The matrix was modeled as a linear isotropic elastic material with Young's modulus $E^m = 3.31$ GPa and Poisson's ratio $v^m = 0.35$, and the fiber was modeled as a linear transversely isotropic elastic material with longitudinal Young's modulus $E_1^f = 303$ GPa, transverse Young's modulus $E_2^f = 15.2$ GPa, longitudinal Poisson's ratio $v_{12}^f = 0.2$, transverse Poisson's ratio $v_{23}^f = 0.2$, and longitudinal shear modulus $G_{12}^f = 9.65$ GPa. A variety of elastic RVEs with three different fiber arrangements, i.e., square array, diamond array and hexagonal array, were generated by setting and varying fiber volume fraction V_f from 0.1 to 0.6 using the *Viscoelastic RVE Calculator* and the effective material properties are calculated and compared to that of elastic FE-RVE with random fiber distribution taken from [29] in Fig. 5. It is shown that, overall, in each subplot, predictions from three model calculations with different fiber arrangement agree fairly well, but some deviations still exist in particular cases, which reflects the effect of fiber arrangement. For effective longitudinal Young's modulus E_1, longitudinal Poisson's ratio v_{12}, and longitudinal shear modulus G_{12}, the values predicted by the three models are all in excellent agreement with that noted by random fiber distribution, which indicates that fiber arrangement has a negligible effect on the these three effective longitudinal material properties. In contrast, for effective transverse material properties such as transverse Young's modulus E_2, transverse Poisson's ratio v_{23}, and transverse shear modulus G_{23}, the values predicted by the hexagonal array agree very well with those by the random array, while slight deviations are observed in the square and diamond array.

4.2. Calculation of effective relaxation properties for viscoelastic RVE

Next, to further validate the functionality of the tools for predicting effective relaxation modulus of viscoelastic composites, we calculated the orthotropic stress-relaxation behavior of viscoelastic RVE using the *Viscoelastic RVE Calculator* plug-in, and then we implemented the effective viscoelastic properties into a user-defined material subroutine UMAT for homogenization. In this benchmark case, the fiber is modeled as an isotropic and linear elastic material with Young's modulus $E^f = 80$GPa and Poisson's ratio $v^f = 0.3$, and the matrix is modeled as an isotropic and linear viscoelastic material with a constant Poisson's ratio $v^m = 0.4$ and relaxation modulus expressed in Eq. 3 by $E_\infty^m = 4$GPa, $E_1^m = 4$ GPa, and $\tau_1 = 30$. The fiber volume fraction is set to 0.2 and the fiber is arranged in square array. By taking the constituent material properties as input into the plug-in, the six independent coefficients of the effective stiffness matrix for the viscoelastic composites $C_{11}(t), C_{12}(t), C_{22}(t), C_{23}(t), C_{44}(t)$, and $C_{55}(t)$ are calculated as output. The independent coefficients $C_{ij}(t)$ predicted by the *Viscoelastic RVE calculator* plug-in are subsequently determined as a function of time and the time history of each independent stiffness matrix coefficient $C_{ij}(t)$ is fitted to Eq. 12 using the leastsq function from Python's scipy.optimize library, and the Prony coefficients for each coefficient $C_{ij}(t)$ are listed in Table 2. The consistent Jacobin matrix is then readily available as described in Section 3.2. A homogeneous domain with equivalent orthotropic viscoelastic properties is therefore defined through a user defined material subroutine UMAT. The computed relaxation results predicted by the *Viscoelastic RVE Calculator* plug-in and UMAT are given in Fig. 6. Recently, Rodríguez-Ramos et al. [24] formulated a closed-form theory for computation of the relaxation effective moduli for fibrous viscoelastic composites using the asymptotic homogenization method (AHM) [25,26,23], and the theoretical results predicted by AHM are also plotted here for comparison. As can be seen that all results agree very well with each other.

In addition, Fig. 6 also gives as inserted figures the deformed mesh with contour of von Mises stress distribution. It is clearly seen that the uniformly unit cell with homogeneous material properties defined by UMAT deforms homogeneously and exhibits a similar response over the entire domain, while the mesh of two-material RVE exhibits significantly different stress spatially due to the heterogeneous material definition of the matrix and fiber phases. Finally, it can be concluded that the one-material homogeneous model defined by the UMAT yields equivalent homogeneous relaxation response out of relaxation data obtained by the two-material defined RVE in the plug-in. We note that from the point of view of mechanics of composites, our plug-in software provides functionalities for finding the average orthotropic viscoelastic properties of a single unidirectional lamina from the known properties of the constituent materials and the microstructure geometry. This procedure is referred to as *micromechanics* of a lamina. The relaxation constitutive relations for a unidirectional lamina are subsequently developed and implemented into a UMAT subroutine, by which the lamina is modeled as a homogeneous layer. This is called the *macromechanics* of a lamina. A true composite structure generally consists of laminates containing various laminas stacked on each other. Knowing the macromechanics of single unidirectional lamina, one could further develop the macromechanics of a laminate by calculating the ABD matrix [41,17]. This

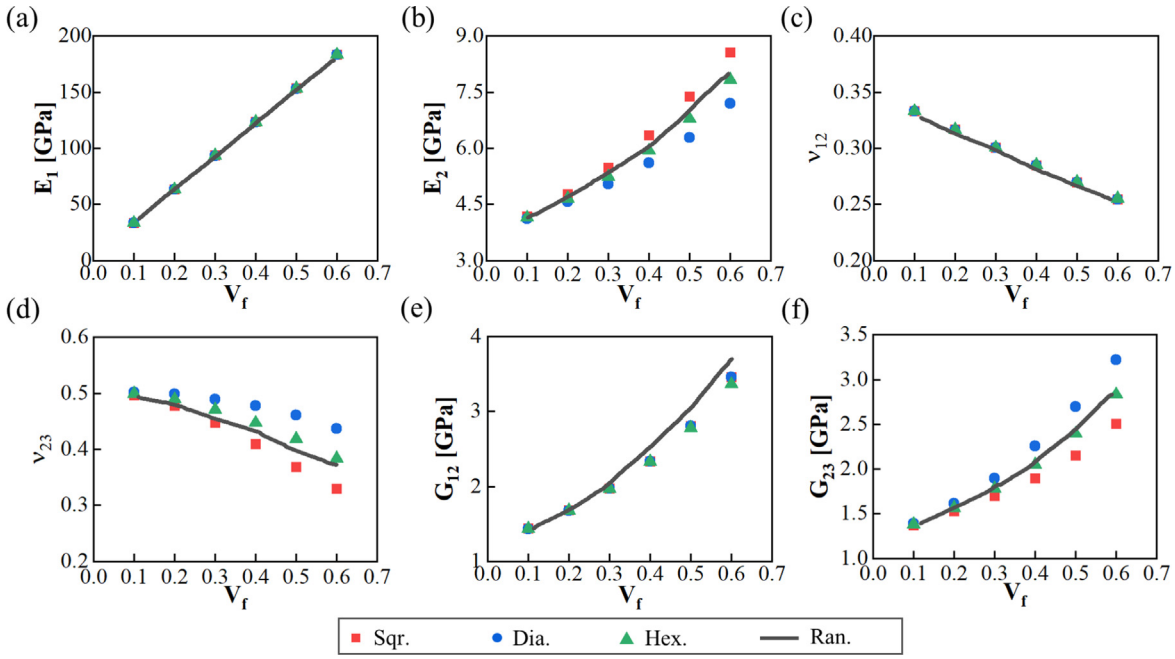

Fig. 5. Comparison of the plug-in calculated effective elastic material properties with three different fiber arrangements, i.e., square array, diamond array and hexagonal array, to random fiber distribution results extracted from [29], according to fiber volume fraction V_f. (a) longitudinal Young's modulus E_1, (b) transverse Young's modulus E_2, (c) longitudinal Poisson's ratio ν_{12}, (d) transverse Poisson's ratio ν_{23}, (e) longitudinal shear modulus G_{12}, (f) transverse shear mod.ulus G_{23}.

Table 2
Prony coefficients (in GPa) and relaxation time (in second) for the viscoelastic RVE.

k	$C_{11,k}$	$C_{12,k}$	$C_{22,k}$	$C_{23,k}$	$C_{44,k}$	$C_{55,k}$	τ_k
0	32.38	13.20	21.56	13.40	3.71	4.00	-
1	8.03	6.37	10.38	6.48	1.81	1.92	30

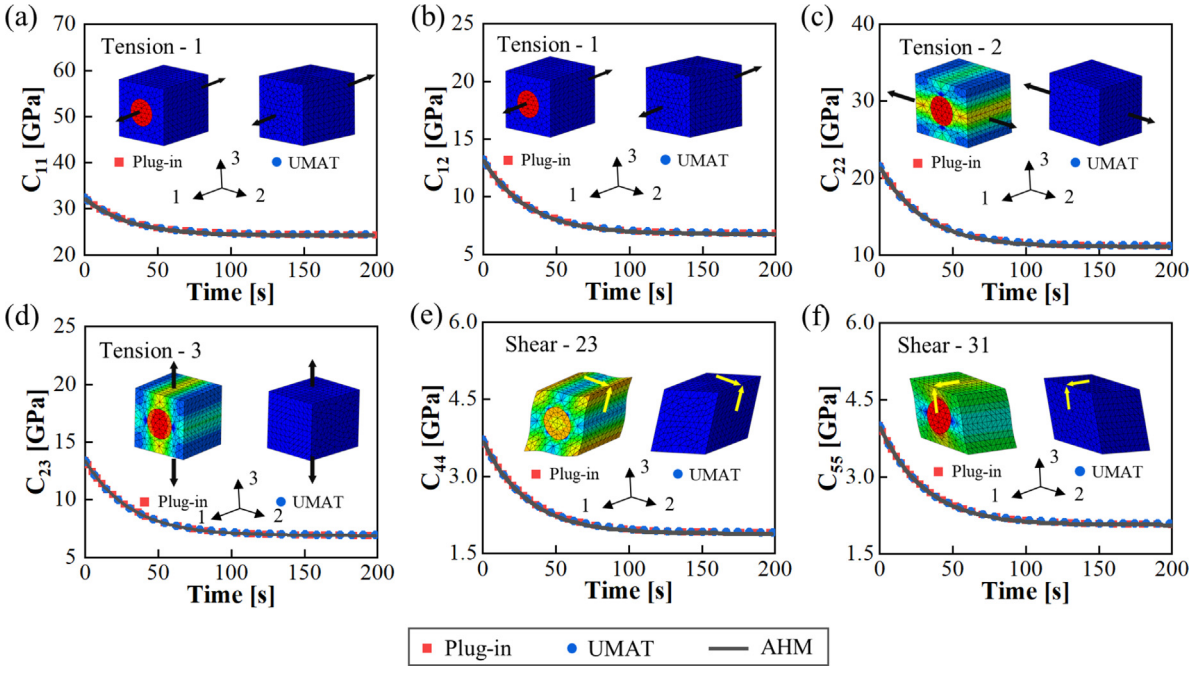

Fig. 6. Variation of effective stress relaxation stiffness matrix coefficients $C_{ij}(t)$ as a function of time predicted by the *Viscoelastic RVE Calculator* plug-in, UMAT and AHM [24]. (a) C_{11}, (b) C_{12}, (c) C_{22}, (d) C_{23}, (e) C_{44}, and. (f) C_{55}.

knowledge will form the basis for the mechanical design of general structures made of composite materials.

4.3. Effect of fiber arrangement and environmental temperature

Having solved the benchmark problems and validated the accuracy of the proposed analysis tools, we then move on to apply the tools to analyze the effect of RVE microstructure geometry, i.e., fiber volume fraction and fiber arrangement, as well as environmental temperature on the average orthotropic relaxation properties of viscoelastic composites. A real-world engineering example was considered in this case. The fiber and matrix properties are obtained from experimental tests of real samples in the literature [18,20]. The fiber is assumed as linear elastic and transversely isotropic, and the properties are $E_1^f = 233$ GPa, $E_2^f = E_3^f = 15$ GPa, $G_{12}^f = G_{13}^f = 8.963$ GPa, $G_{23}^f = 5.639$ GPa, $v_{12}^f = v_{13}^f = 0.2$, and $v_{23}^f = 0.33$. For the matrix, the relaxation times and Prony coefficients at the reference temperature $T_0 = 40^\circ$C are given in Table 3. The matrix properties are expressed in terms of relaxation times and Prony coefficients in Eq. 3, and a constant Poisson's ratio 0.33 is assumed. To capture the temperature effect on the relaxation behavior, the temperature shift factor is adopted in terms of the Williams-Landel-Ferry (WLF) equation in Eq. 6, and the material constants C_1 and C_2 were set to $C_1 = 28.3816$ and $C_2 = 93.291$.

We began by analyzing the effect of RVE geometry parameters such as fiber volume fraction and fiber arrangement on the average orthotropic properties of viscoelastic RVEs. This problem was previously studied by Kwok et al. [18] and Liu et al. [20] by using different methods, however, in previous studies the difference between various fiber arrangements (i.e., square array, diamond array and hexagonal array) was ignored, and only the relaxation properties of a particular viscoelastic RVE characterized by the square array and a fixed fiber volume fraction $V_f = 0.64$ were predicted. Here, taking advantage of the developed software tools, we report a parametric study of RVE geometry including three different fiber arrangements and predict the average relaxation behavior for these RVEs at a variety of fiber volume fractions and environmental temperatures. Fig. 7 gives the relaxation results for RVEs containing different fiber arrangements at three volume fractions of $V_f = 0.2, 0.4, 0.64$ when environment temperature is kept constant and equal to the reference temperature 40°C. It is shown that for C_{11}, C_{12}, C_{22} and C_{55} the relaxation results are almost unaltered by variations in fiber arrangement. By contrast, for C_{23} and C_{44} reasonable deviations exist among the three sets of data. Specifically, the relaxation curve for RVE with hexagonal fiber array is located in the middle of the three sets of data, and a higher value can be observed in diamond array and lower in square array, and the deviation is found to increase with the increase of fiber volume fraction. We would also note that in such a real engineering problem, C_{11} has a much weaker time dependence than the other moduli which is attributed to the fact that the behavior in fiber direction is dominated strongly by the time-independent behavior of the fibers. We next proceed to analyze the effect of environmental temperature on the relaxation behavior of composites by specifying a fixed fiber volume fraction. Toward this end, in Fig. 8 we report the relaxation results for RVEs characterized by same fiber volume fraction of 0.64 under various environmental temperatures such as 30 °C, 40 °C and 50 °C. It can be seen in this figure that the relaxation process of a composite material would be accelerated by a higher experimental temperature, while a lower experimental temperature would delay the relaxation process.

5. Application to composite tape-spring hinges

So far we have developed analysis tools that capable of predicting the elastic or viscoelastic behavior of single unidirectional composite lamina through micromechanics RVE analysis and we have shown that the tools are efficiently applicable to a variety of different situations in terms of fiber arrangement, fiber volume fraction, and environmental temperature. Although we have demonstrated the mechanics of a lamina with unidirectional fibers, it is important to point out that our approach can be extended to analyze the viscoelastic relaxation of general laminated structures that consist of various laminas stacked on each other. In this section we focus on deployable composite tape-spring hinge [see Fig. 1 (a)] and use the proposed analysis tools to reveal the effect of viscoelastic relaxation on its deployment dynamics. Fig. 9 shows the geometry of the composite tape-spring hinge being considered in this work. A specimen was usually manufactured by laying multiple plies of carbon fiber fabric impregnated with epoxy resin on a mandrel for curing. After cooling, the mandrel was pulled out and two opposite parallel slots were cut by machine to obtain the final geometry as depicted in Fig. 9. In the subsequent test, the tape spring hinge specimen was first folded and stored for a given length of time and then deployed by releasing one of the ends, while the shape change during deployment was recorded with a high-speed camera. More details about fabrication and test of this structure can be found in Refs. [15,18,21]. In this study we will focus on the numerical modeling of deployment dynamics of composite tape-spring hinge with time-dependent viscoelastic relaxation effect accounted for.

The core of the modeling consists of definition of the relaxation in material properties during the storage time period after folding and before deployment. However, it is computationally impracticable to explicitly simulate the relaxation behavior of a complex laminated composite structure in its natural time scale since the storage time is usually very long (on the order of months or even years). Here we employ a technique recently proposed by Fernandes et al. [21] and simulate the relaxation of material properties by using a set of distinct fictitious temperatures. First, we remind that the time- and temperature-dependent properties of a particular unidirectional lamina (characterized by a fiber volume fraction of 0.64 and hexagonal array) are readily identified from Fig. 8. In Table 4 we list the material properties of a lamina at the initial state and after being stowed at 50°C for 1 month, 1 year and 2 years, respectively. Each set of lamina properties in Table 4 is related to a distinct fictitious temperature, and the relaxation of the material properties will be achieved by specifying a change in the fictitious temperature. It should be pointed out that the fictitious temperature does not represent the physical temperature of the specimen and its change does not result in geometrical variations resulting from thermal-related phenomena. Instead, the change of this fictitious temperature causes the numerical model to update the material properties of the composite from an unrelaxed state to a relaxed state, which shall be equivalent to the relaxation observed due to an extended period of storage [21].

Table 3
Prony coefficients and relaxation times for PMT-F4 epoxy matrix at the reference temperature $T_0 = 40^\circ$C.

i	∞	1	2	3	4	5	6	7
E_i^m [MPa]	1000	224.1	450.8	406.1	392.7	810.4	203.7	1486.0
τ_i [s]	-	1.0e3	1.0e5	1.0e6	1.0e7	1.0e8	1.0e9	1.0e10

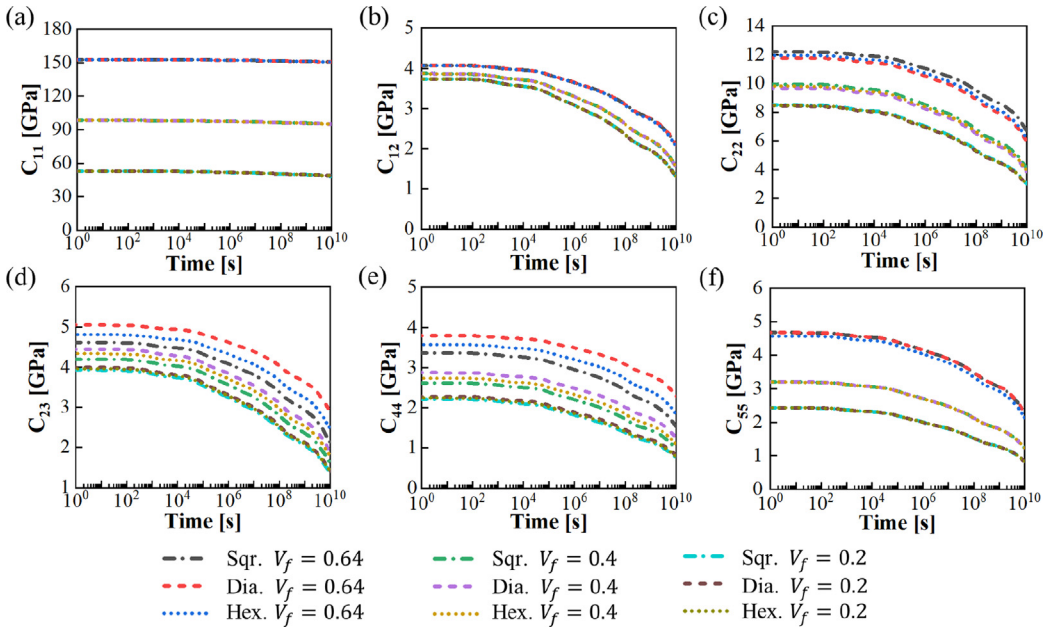

Fig. 7. Variation of average relaxation stiffness matrix coefficients $C_{ij}(t)$ as a function of time for viscoelastic RVEs characterized by different fiber arrangements and fiber volume fraction. The environmental temperature is assumed as $T = 40$°C. (a) C_{11}, (b) C_{12}, (c) C_{22}, (d) C_{23}, (e) C_{44}, and (f) C_{55}.

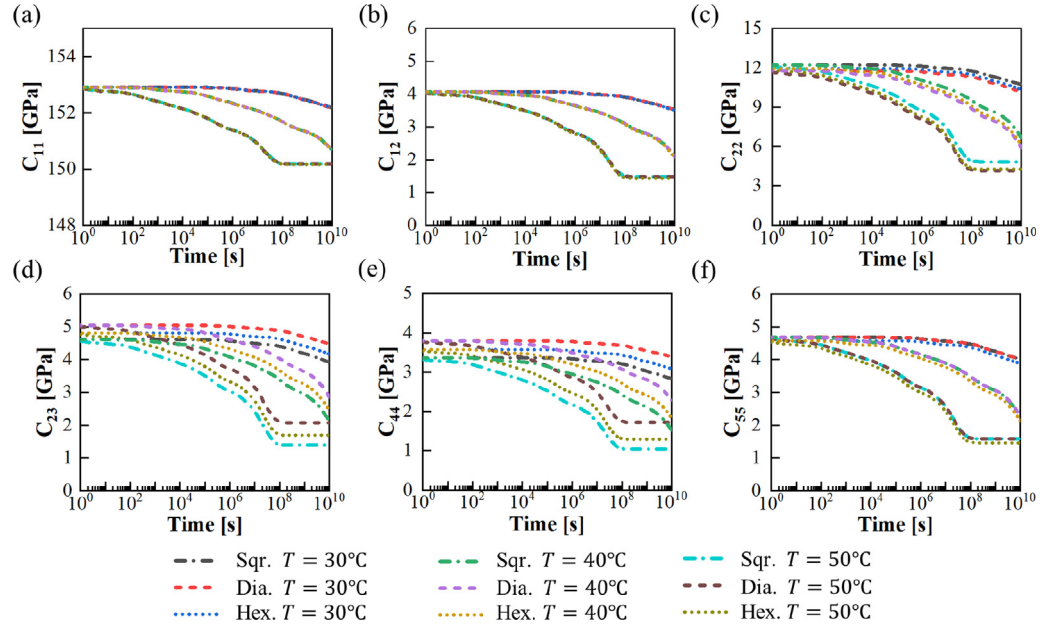

Fig. 8. Variation of average relaxation stiffness matrix coefficients $C_{ij}(t)$ as a function of time for viscoelastic RVEs characterized by different fiber arrangements and environmental temperatures. The fiber volume fraction is assumed as $V_f = 0.64$. (a) C_{11}, (b) C_{12}, (c) C_{22}, (d) C_{23}, (e) C_{44}, and (f) C_{55}.

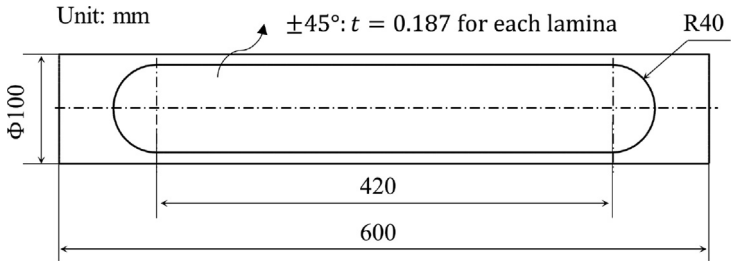

Fig. 9. (a) Geometry of composite tape-spring hinge with dimensions (front view).

Table 4
Estimated material properties of a unidirectional lamina after 1 month, 1 year and 2 years of relaxation at a temperature of 50 °C.

Relaxation time	$E_1[GPa]$	$E_2, E_3[GPa]$	v_{12}, v_{13}	v_{23}	$G_{12}, G_{13}[GPa]$	$G_{23}[GPa]$	Fictitious temperature
Initial	150.93	9.99	0.24	0.4	4.58	3.58	T_0
1 month	149.97	6.57	0.24	0.4	2.84	2.35	T_1
1 year	149.58	4.29	0.24	0.4	1.77	1.54	T_2
2 years	149.50	3.73	0.24	0.4	1.52	1.34	T_3

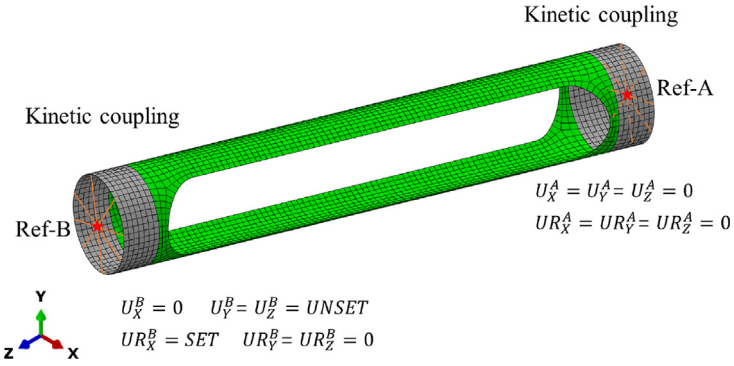

Fig. 10. Finite element model of composite tape-spring hinge with boundary conditions and loads.

Fig. 10 presents a finite element mesh representation for the composite tape-spring hinge with boundary conditions and loads. The finite element model was constructed using four-node reduced integration general-purpose shell elements with enhanced hourglass control (element type: S4R) in the commercial package Abaqus/Explicit 2020. Rigid cross-sections are formed by kinematically coupling the nodes at two end regions (shown in grey in Fig. 10)) to two reference points, Ref-A and Ref-B, respectively. To simulate the complete test procedure [21], each simulation run consists of two steps, where the first step generates the folded configuration of the hinge, and the second step simulates its dynamic deployment. In the first step, all six degrees of freedom of the reference point A were restrained, defining a clamped condition, whereas for the reference point B two translational degrees of freedom along Y and Z were left free and a prescribed rotational angle was applied along X to induce folding of the hinge. The initial fictitious temperature of T_0 was applied to the entire structure. The hinge was folded over 180° with the initial material properties in a quasi-static manner, resulting in a fully folded configuration from which the subsequent deployment initiates. In the deployment step, a change in fictitious temperature was induced, and in the meantime the boundary conditions applied to reference point B were removed instantaneously while the reference point A remained clamped. As a result, the hinge was allowed to deploy at a degraded material state. It is important to point out that on contrary to the folding simulation, where the simulation time had no physical meaning but was simply determined such that the kinetic energy would be negligible in the folding process, in the deployment analysis the simulation time is the actual physical time over which the motion occurs and so it is important to switch to a realistic model of the actual damping of the structure [15]. Hence, in our simulations, a small viscous pressure load was applied over the entire surface of the hinge throughout the folding and deployment to simulate the air friction effect; the viscosity coefficient was determined through a trial and error process to better match the experimental results and was set to 1.5×10^{-8}. The density of the composite materials was set to 1580.76 kg/m^3 and a gravity load was defined over the whole structure, in the negative Z direction, throughout the analysis.

In order to validate the numerical model, we start by considering the deployment dynamics of the composite tape-spring hinge that is deployed immediately after folding and without storage. The initial material properties in Table 4 were used throughout the whole simulation steps including folding and deployment. Fig. 11(a) gives the evolution of deployment angle as a function

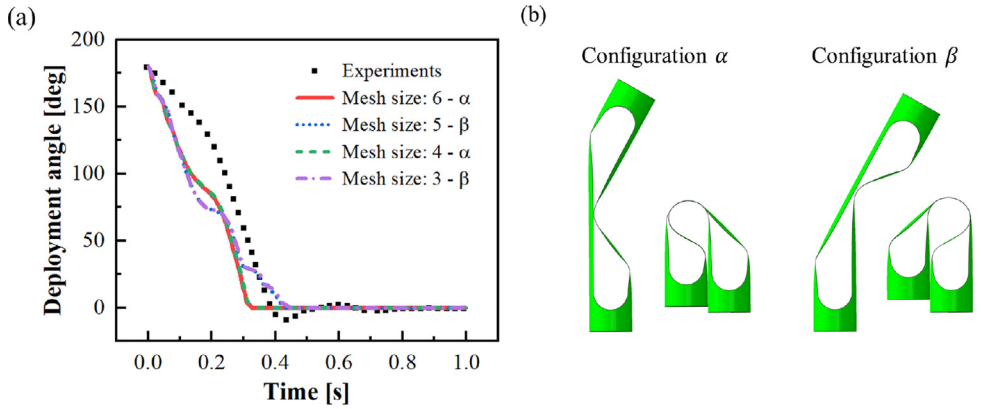

Fig. 11. Deployment dynamics of the composite tape-spring hinge. (a) Experimental and numerical evolution of deployment angle as function of time. The variations in line type correspond to finite element models with different mesh size. The experimental data (square markers) are taken from Ref. [21]. (b) Two different configurations (α and β) formed in the quasi-static .folding process.

of time, where the numerical results (lines) are in good agreement with the experimental data (square markers) reported by Fernandes et al. [21]. It is important to point out that there are two distinct set of deployment angle-time response curves that randomly occur in the simulations. This is attributed to the variability in configuration of the hinge formed in the folding process, as shown in Fig. 11(b). These two possible equilibrium folding paths, which were previously reported by experimental observations in Ref. [15], are reproduced in our simulations by adjusting the mesh size of the finite element model. We would like to note that one of the two configurations occurs with same probability in principle, and in numerical practice the variability may be affected by rounding errors due to the large number of increments required in the dynamic explicit procedure. More importantly, the dynamic response of the hinge is distinct when the deployment starts from different configurations. Specifically, in the case of configuration α, the hinge is effectively shorter and it will rotate faster in the deployment process. The deployment snapshots from simulations are given in terms of both configurations in Fig. 12, showing a good agreement with the previous reported experimental

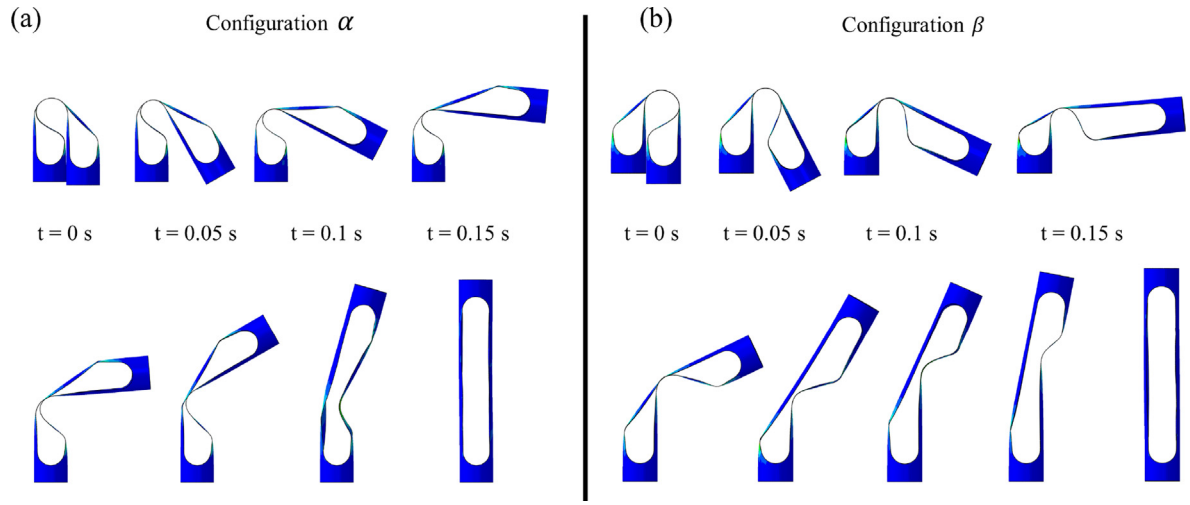

Fig. 12. Deployment snapshots of the composite tape-spring hinge when the deployment starts from fully folded (a) configuration α and (b) configuration β.

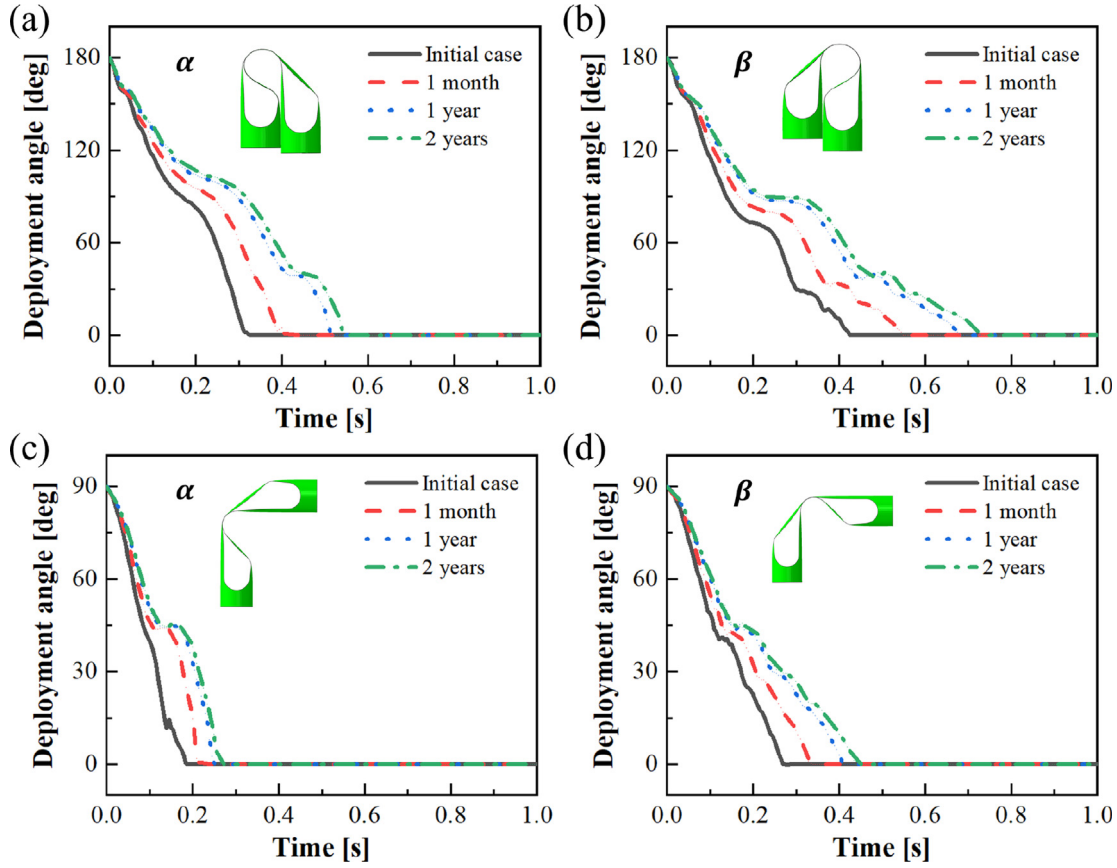

Fig. 13. Deployment angle as function of time for composite tape-spring hinge after being stowed in its fully folded (a) configuration α, (b) configuration β, and half folded (c) configuration α, (d) configuration β, for various relaxation time periods at 50 °C.

observations in Ref. [21]. Finally, the model was applied to simulate the effect of time- and temperature-dependent relaxation on the deployment dynamics of the hinge. A fictitious temperature change was introduced to switch the material properties from initial state to relaxed state in the deployment simulation. Fig. 13 presents the variation of deployment dynamics for the composite tape-spring hinge stored at 50°C for different periods of relaxation. In order to assess the effect of the amount of stowage strain on the viscoelastic behavior, the structure was stowed under two folded states, e.g., fully folded state in 180°, and half folded state in 90°. In general, the simulation results show that whenever the hinge was stowed in its fully or half folded configuration α or β, the deployment of the hinge after stowage is about a fraction of second slower than the initial unrelaxed case and the longer the storage time the slower the deployment rotation, which agrees with the findings of Fernandes et al. [21]. We acknowledge that this research focuses only on the simulation and theoretical prediction for the relaxation behavior of non-ageing linear viscoelastic composite materials, further developments of the present work will include the extension to ageing viscoelastic composite materials, and validation of simulations to experimental results.

6. Conclusion

Fiber-reinforced polymer composites exhibit more or less modulus relaxation behavior due to the inherent viscoelasticity of polymers. Knowledge of their viscoelastic behavior is essential to achieve optimal design of the composites, especially for the design of stored strain energy deployable structures in the aerospace industry.

In the present paper, we proposed a finite element (FE) based two-scale computational strategy that capable of evaluating the viscoelastic behavior of unidirectional composite laminates and general shell structures. At microscale, a numerical analysis tool is developed and linked with Abaqus/CAE via a graphical user interface plug-in called *Viscoelastic RVE calculator* herein, which provides capabilities for calculating the orthotropic viscoelastic properties of unidirectional composites by taking the microstructure geometry and the known properties of constituent materials as input. A parametric study on the effect of microstructure geometry and environmental temperature on the viscoelastic response of unidirectional composites was conducted by taking advantage of the efficiency of the tool. It is shown that the relaxation curve for composites with hexagonal fiber array is always intermediate between the curves obtained in the square and diamond array; and unsurprisingly, the relaxation process would be accelerated by a higher experimental temperature and delayed by a lower one. We also show that the time-dependent lamina properties output by the plug-in can be subsequently used to model the viscoelastic behavior of composite laminates at macroscale with the help of Abaqus built-in functions to define the stacking sequence and accordingly update the material properties. Particularly, we formulated a 3D shell FE model and quantified the effect of long-term stowage on the deployment dynamics of composite tape-spring hinge to demonstrate the strategy. It is shown, in good agreement with previous experimental works, that the long-term stowage would lead to a significant decrease in the deployment rate of the hinge when compared to the unstored case.

We would like to note that all the source codes of the plug-in tool as well as the Abaqus scripts are made available to the community, alleviating the burdens of multi-scale viscoelasticity analysis of composite laminates and shell structures. This also makes *Viscoelastic RVE Calculator* an open-source tool that enables developers to customize the software for specific purposes. We also expect our multiscale computational strategy to be applied to analyze the viscoelastic behavior of more general thin-walled composite laminated structures such as composite lenticular tubes [42], triangular rollable and collapsible booms [43], and other foldable thin shell space structures [4,44].

7. Data availability

The source codes of the plug-in tool as well as the benchmark scripts are published open-source and can be downloaded from https://github.com/Dr-Ning-An/Viscoelastic-RVE-Calculator

Declaration of Competing Interest

The authors declare that they have no known competing financial interests or personal relationships that could have appeared to influence the work reported in this paper.

Acknowledgement

This research was supported by the Fundamental Research Funds for the Central Universities (No. YJ2021137), the Open Project of State Key Laboratory for Strength and Vibration of Mechanical Structures, Xi'an Jiaotong University (No. SV2021-KF-04), and National Natural Science Foundation of China (No. 11972277). Q. J. acknowledges the support from Shanghai Rising-Star Program (19QB1404000). We also thank Dr. Sadik Omairey of Brunel University London for providing the source codes of EasyPBC.

Appendix A. Supplementary material

Supplementary data associated with this article can be found, in the online version, at https://doi.org/10.1016/j.matdes.2022.110754.

References

[1] Y. Hu, W. Chen, J. Gao, J. Hu, G. Fang, F. Peng, A study of flattening process of deployable composite thin-walled lenticular tubes under compression and tension, Compos. Struct. 168 (2017) 164–177.
[2] J.-B. Bai, D. Chen, J.-J. Xiong, R.A. Shenoi, Folding analysis for thin-walled deployable composite boom, Acta Astronaut. 159 (2019) 622–636.
[3] A.J. Lee, J.M. Fernandez, Inducing bistability in collapsible tubular mast booms with thin-ply composite shells, Compos. Struct. 225 (2019) 111166.
[4] A. Pedivellano, S. Pellegrino, Deployment dynamics of foldable thin shell space structures, in: AIAA Scitech 2021 Forum, 2021, p. 0299.
[5] J. Bai, R. Shenoi, J. Xiong, Thermal analysis of thin-walled deployable composite boom in simulated space environment, Compos. Struct. 173 (2017) 210–218.
[6] G. De Zanet, A. Viquerat, Thermal response of cfrp deployable tubes in the space environment, in: AIAA Scitech 2020 Forum, 2020, p. 1439.
[7] A.I. Khan, E.C. Borowski, E.M. Soliman, M.M. Reda Taha, Examining energy dissipation of deployable aerospace composites using matrix viscoelasticity, J. Aerosp. Eng. 30 (5) (2017) 04017040.
[8] B. Adamcik, J. Firth, M. Pankow, J.M. Fernandez, Impact of storage time and operational temperature on deployable composite booms, in: AIAA Scitech 2020 Forum, 2020, p. 1183.
[9] J.E. Salazar, J.M. Fernandez, Experimental characterization of the dimensional stability of deployable composite booms during stowage, in: AIAA Scitech 2021 Forum, 2021, p. 0195.
[10] J.H. Kang, J.A. Hinkley, K.L. Gordon, S.A. Thibeault, R.G. Bryant, J.M. Fernandez, W.K. Wilkie, H.E.D. Morales, D.E. Mcgruder, R.S. Peterson, et al., Viscoelastic characterization of polymers for deployable composite booms, Adv. Space Res. 67 (9) (2021) 2727–2735.
[11] M. Pathan, V. Tagarielli, S. Patsias, Numerical predictions of the anisotropic viscoelastic response of uni-directional fibre composites, Compos. Part A: Appl. Sci. Manuf. 93 (2017) 18–32.
[12] Z. Yang, H. Wang, X. Ma, F. Shang, Y. Ma, Z. Shao, D. Hou, Flexural creep tests and long-term mechanical behavior of fiber-reinforced polymeric composite tubes, Compos. Struct. 193 (2018) 154–164.
[13] W. Klimm, K. Kwok, Surface accuracy of viscoelastic composite thin-shell deployable reflector antennas, in: AIAA Scitech 2020 Forum, 2020, p. 0932.
[14] K. Kwok, S. Pellegrino, Folding, stowage, and deployment of viscoelastic tape springs, AIAA J. 51 (8) (2013) 1908–1918.
[15] H. Mallikarachchi, S. Pellegrino, Deployment dynamics of ultrathin composite booms with tape-spring hinges, J. Spacecraft Rock. 51 (2) (2014) 604–613.

[16] J. Block, M. Straubel, M. Wiedemann, Ultralight deployable booms for solar sails and other large gossamer structures in space, Acta Astronaut. 68 (7) (2011) 984–992.
[17] J. Gao, W. Chen, B. Yu, P. Fan, B. Zhao, J. Hu, D. Zhang, G. Fang, F. Peng, A multi-scale method for predicting abd stiffness matrix of single-ply weave-reinforced composite, Compos. Struct. 230 (2019) 111478.
[18] K. Kwok, S. Pellegrino, Micromechanics models for viscoelastic plain-weave composite tape springs, Aiaa J. 55 (1) (2017) 309–321.
[19] X. Liu, K. Rouf, B. Peng, W. Yu, Two-step homogenization of textile composites using mechanics of structure genome, Compos. Struct. 171 (2017) 252–262.
[20] X. Liu, T. Tang, W. Yu, R.B. Pipes, Multiscale modeling of viscoelastic behaviors of textile composites, Int. J. Eng. Sci. 130 (2018) 175–186.
[21] P. Fernandes, B. Sousa, R. Marques, J.M.R. Tavares, A. Marques, R.N. Jorge, R. Pinto, N. Correia, Influence of relaxation on the deployment behaviour of a cfrp composite elastic–hinge, Compos. Struct. 259 (2021) 113217.
[22] T. Tang, S.D. Felicelli, Computational evaluation of effective stress relaxation behavior of polymer composites, Int. J. Eng. Sci. 90 (2015) 76–85.
[23] J. Otero, R. Rodríguez-Ramos, R. Guinovart-Díaz, O.L. Cruz-González, F. Sabina, H. Berger, T. Böhlke, Asymptotic and numerical homogenization methods applied to fibrous viscoelastic composites using prony's series, Acta Mech. 231 (7) (2020) 2761–2771.
[24] R. Rodríguez-Ramos, J. Otero, O. Cruz-González, R. Guinovart-Díaz, J. Bravo-Castillero, F. Sabina, P. Padilla, F. Lebon, I. Sevostianov, Computation of the relaxation effective moduli for fibrous viscoelastic composites using the asymptotic homogenization method, Int. J. Solids Struct. 190 (2020) 281–290.
[25] O. Cruz-González, R. Rodríguez-Ramos, J. Otero, A. Ramírez-Torres, R. Penta, F. Lebon, On the effective behavior of viscoelastic composites in three dimensions, Int. J. Eng. Sci. 157 (2020) 103377.
[26] O. Cruz-González, A. Ramírez-Torres, R. Rodríguez-Ramos, J. Otero, R. Penta, F. Lebon, Effective behavior of long and short fiber-reinforced viscoelastic composites, Appl. Eng. Sci. 6 (2021) 100037.
[27] C.-T. Sun, R.S. Vaidya, Prediction of composite properties from a representative volume element, Compos. Sci. Technol. 56 (2) (1996) 171–179.
[28] Z. Xia, Y. Zhang, F. Ellyin, A unified periodical boundary conditions for representative volume elements of composites and applications, Int. J. Solids Struct. 40 (8) (2003) 1907–1921.
[29] Y. Huang, K.K. Jin, S.K. Ha, Effects of fiber arrangement on mechanical behavior of unidirectional composites, J. Compos. Mater. 42 (18) (2008) 1851–1871.
[30] R. Haj-Ali, A. Muliana, A micro-to-meso sublaminate model for the viscoelastic analysis of thick-section multi-layered frp composite structures, Mech. Time-dependent Mater. 12 (1) (2008) 69–93.
[31] K.-K. Jin, Y. Huang, Y.-H. Lee, S.K. Ha, Distribution of micro stresses and interfacial tractions in unidirectional composites, J. Compos. Mater. 42 (18) (2008) 1825–1849.
[32] Z. Wang, D.E. Smith, Numerical analysis on viscoelastic creep responses of aligned short fiber reinforced composites, Compos. Struct. 229 (2019) 111394.
[33] M. Pathan, S. Ponnusami, J. Pathan, R. Pitisongsawat, B. Erice, N. Petrinic, V. Tagarielli, Predictions of the mechanical properties of unidirectional fibre composites by supervised machine learning, Scient. Rep. 9 (1) (2019) 1–10.
[34] Y. Chen, Z. Zhao, D. Li, Z. Guo, L. Dong, Constitutive modeling for linear viscoelastic fiber-reinforced composites, Compos. Struct. 263 (2021) 113679.
[35] F. Ye, H. Wang, A simple python code for computing effective properties of 2d and 3d representative volume element under periodic boundary conditions, arXiv preprint arXiv:1703.03930.
[36] D. Systèmes, Micromechanics Plugin for Abaqus/CAE. Version 1.15-12/11/2017 ed.
[37] S.L. Omairey, P.D. Dunning, S. Sriramula, Development of an abaqus plugin tool for periodic rve homogenisation, Eng. Comput. 35 (2) (2019) 567–577.
[38] L. Riaño, Y. Joliff, An abaqus plug-in for the geometry generation of representative volume elements with randomly distributed fibers and interphases, Compos. Struct. 209 (2019) 644–651.
[39] S.P. Marques, G.J. Creus, Computational viscoelasticity, Springer Science & Business Media, 2012.
[40] E.J. Barbero, Finite element analysis of composite materials using AbaqusTM, CRC Press, 2013.
[41] A. Kueh, S. Pellegrino, Abd matrix of single-ply triaxial weave fabric composites, in: 48th AIAA/ASME/ASCE/AHS/ASC Structures, Structural Dynamics, and Materials Conference, 2007, p. 2161.
[42] Q. Jia, N. An, X. Ma, J. Zhou, Exploring the design space for nonlinear buckling of composite thin-walled lenticular tubes under pure bending, Int. J. Mech. Sci. 207 (2021) 106661.
[43] J.M. Fernandez, C.E. Volle, Corrugated rollable tubular booms, in: AIAA Scitech 2021 Forum, 2021, p. 0296.
[44] T.W. Murphey, Deformable structures collapsible tubular mast (ctm), uS Patent App. 17/171,184 (Jun. 3 2021).